Structure and magnetic properties of binuclear Cu2(O2CCHCHCH3)4(DMF)2: a carboxylate-bridged Cu(II) spin dimer

ARTICLE *in* INORGANICA CHIMICA ACTA · DECEMBER 2000

Impact Factor: 2.05 · DOI: 10.1016/S0020-1693(00)00288-7

ELSEVIER

www.elsevier.nl/locate/ica

Inorganica Chimica Acta 310 (2000) 81–88

Inorganica Chimica Acta

Structure and magnetic properties of binuclear $Cu_2(O_2CCH{=}CHCH_3)_4(DMF)_2$: a carboxylate-bridged Cu(II) spin dimer

Roxana F. Schlam [a], Mireille Perec [b], Rafael Calvo [c], Luis Lezama [d], Maite Insausti [d], Teofilo Rojo [d], Bruce M. Foxman [a,*]

[a] *Department of Chemistry, Brandeis University, Waltham, MA 02454-9110, USA*
[b] *Departamento de Química Inorgánica, INQUIMAE, Universidad de Buenos Aires, Ciudad Universitaria, 1428 Buenos Aires, Argentina*
[c] *Departamento de Física, Facultad de Bioquímica y Ciencias Biológicas, Universidad Nacional del Litoral, and INTEC (CONICET-UNL), Güemes 3450, 3000 Santa Fe, Argentina*
[d] *Departamento de Química Inorgánica, Facultad de Ciencias, Universidad del País Vasco, Apartado 644, 48080 Bilbao, Spain*

Received 24 June 2000; accepted 28 August 2000

Abstract

The complex $Cu_2(O_2CCH{=}CHCH_3)_4(DMF)_2$ was synthesized from $Cu(OH)_2$, *trans*-2-butenoic acid, and dimethylformamide. An X-ray structure determination showed that the complex has the familiar $Cu_2(O_2CR)_4L_2$ dimer structure. *trans*-2-Butenoate groups in molecules related by a center of symmetry have a short contact between the α-carbon atoms (3.611 Å), suggesting a study of the solid-state reactivity of this complex. Irradiation of the complex (^{60}Co X-rays, 219 kGy), did not produce any detectable product. Magnetic susceptibility measurements in the range between 2 and 350 K in a powder sample, and EPR measurements in powder and single-crystal samples were performed. The data show the dimeric magnetic structure of the compound, with an antiferromagnetic exchange coupling $J/k_B = -220$ K and a fine structure coupling $D/h = -10.04$ GHz within the excited spin triplet. Hyperfine structure with the two Cu nuclei is clearly observed. These results are discussed in terms of the structure.

Keywords: X-ray crystal structures; Magnetic properties; Binuclear complexes; Cu(II) dimer; EPR measurements; Solid state reactivity

1. Introduction

Metal salts and complexes of the *trans*-2-butenoate moiety have been shown to undergo three unique solid-state transformations. Thus, heating sodium *trans*-2-butenoate **1** leads to one of two possible diastereomers of 1-hexene-3,4-dicarboxylate **2** [1], while ^{60}Co γ-irradiation of **1** leads to trimer **3**, one of eight possible diastereomers [2]. Irradiation of the calcium salt leads to cyclodimer **4**, one of four possible diastereomers [3]. In order to explore the possibility of carrying out a solid-state dimerization of *trans*-2-butenoate to form dimer **2** under different conditions and in a different phase, we undertook the preparation of a series of tetracarboxylatodicopper(II) species. The driving force for this study was based on an earlier speculation that solid materials containing such species would have short contacts (–C=C–···–C=C– ≤ 4.2 Å) between the unsaturated groups and hence would be reactive in the solid state [4–6]. This hypothesis was also explored

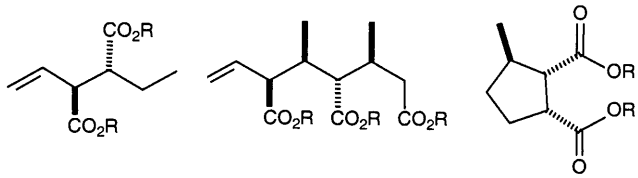

2, R = Na **3**, R = Na **4**, R = $Ca_{0.5}$

* Corresponding author. Tel.: +1-781-736 2532; fax: +1-781-736 2516.
E-mail address: foxman1@brandeis.edu (B.M. Foxman).

0020-1693/00/$ - see front matter
PII: S0020-1693(00)00288-7

using the Cambridge Structural Database [7]. The crystal structure of $Cu_2(O_2CCH{=}CHCH_3)_4(quinoline)_2$ (**5**) showed no alkene–alkene contacts below 5.4 Å [8], presumably owing to the large quinoline groups, while the more compact $Cu_2(O_2CCH_3)_4(OH_2)_2$ (**6**) shows a short methyl–methyl contact (between parallel methyl groups) of 4.28 Å [9], slightly longer than the usual distance generally considered to be the maximum for a radiation- or photochemically-induced solid-state reaction [6]. Based on the observation that acetate complexes are often useful models for the generation of reactive phases [10], we felt that using an axial group smaller than quinoline might be more effective in the engineering of short contacts between butenoate moieties. Our first attempt, described herein, led to an apparent success in orienting the reactive groups. This paper reports the results of a full structural, chemical and physical characterization of the title complex, including studies of its solid-state reactivity and magnetic properties.

2. Experimental

All reagents were obtained from commercial sources and used without further purification. Elemental analyses were performed with a Carlo Erba EA 1108 analyzer. IR spectra were recorded as KBr disks with a Nicolet 510P FTIR spectrometer. TGA analyses were recorded on a Mettler TG-50 thermal analyzer in a dynamic atmosphere of O_2 at a heating rate of 5°C min^{-1}. A Gammacell 220 Irradiation Chamber (Atomic Energy of Canada) was used for γ-irradiation experiments.

Table 1
Crystallographic data [a] for $Cu_2(O_2CCH{=}CHCH_3)_4(DMF)_2$

Chemical formula	$C_{22}H_{34}O_{10}N_2Cu_2$
Formula weight	613.586
Crystal system	monoclinic
Space group	$P2_1/c$ (no. 14)
T (K)	294
Unit cell dimensions	
a (Å)	9.951(2)
b (Å)	17.433(4)
c (Å)	8.893(4)
β (°)	115.54(3)
V (Å^3)	1392.0(8)
Z	2
ρ_{calc} (g cm^{-3})	1.464
ρ_{obsd} (g cm^{-3})	1.47(2)
λ (Å)	1.54178
μ (mm^{-1})	2.30
Transmission coefficient (empirical correlation)	0.844–0.997
Unique reflections; number observed	1484; 1372 ($I>1.96\sigma(I)$)
R_{av}	0.018
R	0.0239
R_w	0.0287

[a] $R=\Sigma\|\|F_o\|-\|F_c\|\|/\Sigma|F_o|$; $R_w=\{\Sigma w[|F_o|-|F_c|]^2/\Sigma w|F_o|^2\}^{1/2}$; $R_{av}=\Sigma\|\|I_{av}|-|I_o|/\Sigma|I_{av}|$.

2.1. $Cu_2(O_2CCH{=}CHCH_3)_4(DMF)_2$ (7)

Freshly prepared $Cu(OH)_2$ (1.0 g, 10 mmol) was mixed with *trans*-2-butenoic acid (2.0 g, 22 mmol) dissolved in 50 ml of water–ethanol (1:1) at room temperature (r.t.) under stirring. A green–blue solid was collected and immediately washed with small amounts of ethanol, and dried in air. IR (KBr): 1575, 1414 cm^{-1} for $\nu_a(CO_2)$ and $\nu_s(CO_2)$, respectively. The solid was insoluble in water and in most non-coordinating organic solvents. Addition of DMF gave a dark green solution; after a week green crystals of the adduct were removed by filtration, washed with acetone, and dried in vacuum. *Anal.* Calc. for $C_{22}H_{34}O_{10}N_2Cu_2$: C, 43.05; H, 5.60; N, 4.55. Found: C, 43.15; H, 5.60; N, 4.60%. IR (KBr, cm^{-1}): 2965 w, 2938 w, 2911 w, 1655 vs (C=C), 1597 vs ($\nu_a(CO_2)$), 1530 w, 1441 vs, 1418 vs ($\nu_s(CO_2)$), 1395 vs, 1252 m, 1109s, 968 s, 853 m, 737 s, 700 w, 679 m, 465 m, 370 m, 304 m. TGA carried out under an O_2 atmosphere shows two clearly defined steps: (i) 71–133°C, loss of two DMF molecules (approximately 23%); (ii) 207–283°C, combustion of the compound to CuO (residual mass approximately 25% of that of the unheated compound).

2.2. X-ray structure determination

Crystallographic data for compound **7** are summarized in Table 1. Data were collected on a Nonius CAD-4U diffractometer (Cu Kα radiation, $\lambda=1.54178$ Å) [11]. Data were processed using the Nonius MolEN package [12]. During the data collection the crystal decomposed, showing a 27.8% loss in diffracted intensity after 17.6 h exposure to Cu Kα radiation; as a consequence of the rapid decomposition, data collection was terminated at $\theta_{max}=51°$. Absorption and linear decay corrections were applied to the data. The Cu position was obtained from a three-dimensional Patterson map; subsequent difference Fourier syntheses revealed the position of the O, N, C and H atoms. Full-matrix least-squares refinement was carried out using the Oxford University CRYSTALS system [13]. All non-hydrogen atoms were refined using anisotropic displacement parameters. H atoms were fixed at calculated positions, which were updated following each least-squares cycle. Drawings were produced using the Oxford University program CAMERON [14]. Selected bond lengths and angles appear in Table 2. A full report on the structure is available as a CIF file.

Table 2
Selected bond lengths and angles for $Cu_2(O_2CCH{=}CHCH_3)_4(DMF)_2$ [a]

Cu(1)–Cu(1)	2.6126(6)	O(5)–C(9)	1.228(3)
Cu(1)–O(1)	1.953(2)	C(1)–C(2)	1.479(3)
Cu(1)–O(2)′	1.971(2)	C(2)–C(3)	1.307(4)
Cu(1)–O(3)	1.965(2)	C(3)–C(4)	1.479(4)
Cu(1)–O(4)′	1.974(2)	C(5)–C(6)	1.483(4)
Cu(1)–O(5)	2.164(2)	C(6)–C(7)	1.295(4)
O(1)–C(1)	1.259(3)	C(7)–C(8)	1.491(4)
O(2)–C(1)	1.254(3)	C(9)–N(1)	1.318(3)
O(3)–C(5)	1.261(3)	C(10)–N(1)	1.435(4)
O(4)–C(5)	1.253(3)	C(11)–N(1)	1.455(3)
Cu(1)′–Cu(1)–O(1)	85.49(5)	Cu(1)–O(3)–C(5)	123.5(2)
Cu(1)′–Cu(1)–O(2)′	83.31(5)	Cu(1)–O(4)′–C(5)′	122.4(2)
O(1)–Cu(1)–O(2)′	168.79(7)	Cu(1)–O(5)–C(9)	118.5(2)
Cu(1)′–Cu(1)–O(3)	84.07(5)	O(1)–C(1)–O(2)	125.1(2)
O(1)–Cu(1)–O(3)	89.62(7)	O(1)–C(1)–C(2)	116.7(2)
O(2)′–Cu(1)–O(3)	89.45(8)	O(2)–C(1)–C(2)	118.3(2)
Cu(1)′–Cu(1)–O(4)′	84.84(5)	C(1)–C(2)–C(3)	124.8(2)
O(1)–Cu(1)–O(4)′	90.09(7)	C(2)–C(3)–C(4)	125.7(3)
O(2)′–Cu(1)–O(4)′	88.69(8)	O(3)–C(5)–O(4)	125.2(2)
O(3)–Cu(1)–O(4)′	168.90(7)	O(3)–C(5)–C(6)	115.8(2)
Cu(1)′–Cu(1)–O(5)	177.00(5)	O(4)–C(5)–C(6)	119.0(2)
O(1)–Cu(1)–O(5)	97.32(6)	C(5)–C(6)–C(7)	124.4(2)
O(2)′–Cu(1)–O(5)	93.89(7)	C(6)–C(7)–C(8)	126.7(3)
O(3)–Cu(1)–O(5)	94.87(7)	O(5)–C(9)–N(1)	125.6(2)
O(4)′–Cu(1)–O(5)	96.18(7)	C(9)–N(1)–C(10)	121.5(2)
Cu(1)–O(1)–C(1)	122.2(2)	C(9)–N(1)–C(11)	120.7(2)
Cu(1)–O(2)′–C(1)′	124.0(2)	C(10)–N(1)–C(11)	117.7(2)

[a] 'Primed' atoms are related by the symmetry operation $(-x, -y, -z)$

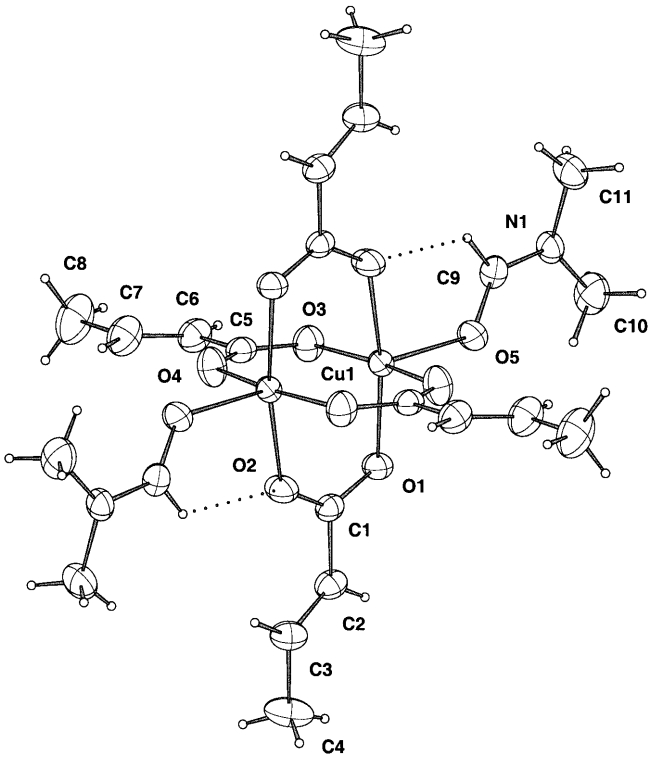

Fig. 1. Molecular structure of $Cu_2(O_2CCH{=}CHCH_3)_4(DMF)_2$ (45% probability ellipsoids).

2.3. Magnetic and EPR measurements

Magnetic susceptibility measurements were performed between 1.8 and 300 K on a powder sample with a Quantum Design MPMS-7 Squid magnetometer. The magnetic field was 0.1 T, where the magnetization versus field curve was still linear at the lowest temperatures T. The experimental values were corrected for the diamagnetic contribution. A Bruker ESP-300 spectrometer working at 34 GHz was used in the EPR measurements. Powdered and single-crystal samples of $Cu_2(O_2CCH{=}CHCH_3)_4(DMF)_2$ were measured at 293 and 100 K. For the single-crystal measurements a face of a single crystal of about $0.5 \times 0.5 \times 0.5$ mm was glued to a KCl sample holder cube obtained by cleavage of a larger single crystal. The a and b axes of the crystal were accurately aligned along the x and y axes of the sample holder. The z axis corresponds to the direction $c^* = a \times b$. This method allows the manipulation of the sample without deterioration, as well as alignment with high accuracy within the magnetic field for the EPR measurements. The sample holder was glued to a horizontal surface on top of a rotating pedestal, so that EPR spectra could be collected with the magnetic field in the $xy = ab$, $zx = c^*a$ and $zy = c^*b$ planes of the sample. The angular uncertainty of the orientation of the magnetic field in the $xyz = abc^*$ system of the sample coordinate axes was less than 2°.

3. Results and discussion

3.1. Structure and reactivity

As expected, $Cu_2(O_2CCH{=}CHCH_3)_4(DMF)_2$ (**7**) has the familiar $Cu_2(O_2CR)_4L_2$ structure (Fig. 1). The Cu–Cu distance, 2.6126(6) Å, compares well with the value for the diaqua complex **6** (2.616 Å), as does the distance to the axial oxygen atom (2.164(2) versus 2.156 Å in **6**). Each DMF moiety is coplanar with a butenoate ligand. This feature is likely a consequence of a weak C(9)–H(91)···O(2) $[-x, -y, -z]$ hydrogen bond, which has an angle of 126.8° and a C(9)···O(2) distance of 3.016 Å.

The closest approach between any unsaturated centers is that between a *pair* of potentially reactive molecules, as shown in Fig. 2(a). Apart from this 'dimer pair' interaction, there are *no* other close approaches less than 5.0 Å between unsaturated centers. The shortest C(4)···C(3) approach in Fig. 2 is 4.752 Å, far too long for a cyclodimerization reaction to occur [3]. This leaves the possibility that the short contact shown in Fig. 2, C(2)···C(2) $[-x+1, -y, -z+1]$ (3.611(5) Å), could lead, via an ene reaction, to a dimer having structure **2**. Heating of **7** to effect a thermal ene reaction was not possible owing to the loss of the DMF at

low temperatures. Irradiation of **7** (^{60}Co γ-rays, 219 kGy), did not produce any detectable product. Further inspection of the distances, using the orbital–orbital separation suggested by Kearsley [15], revealed that the likely interorbital separation is 2.13 Å, 0.33 Å longer than the 1.8 Å proposed by Kearsley as the maximum possible orbital separation for solid-state reactivity. Fig. 2(b) shows that, although the absolute distance between butenoates is short, a lateral displacement apparently leads to an unreactive arrangement. Further studies underway in our laboratory will attempt to favorably perturb this separation through a judicious choice of axial ligands.

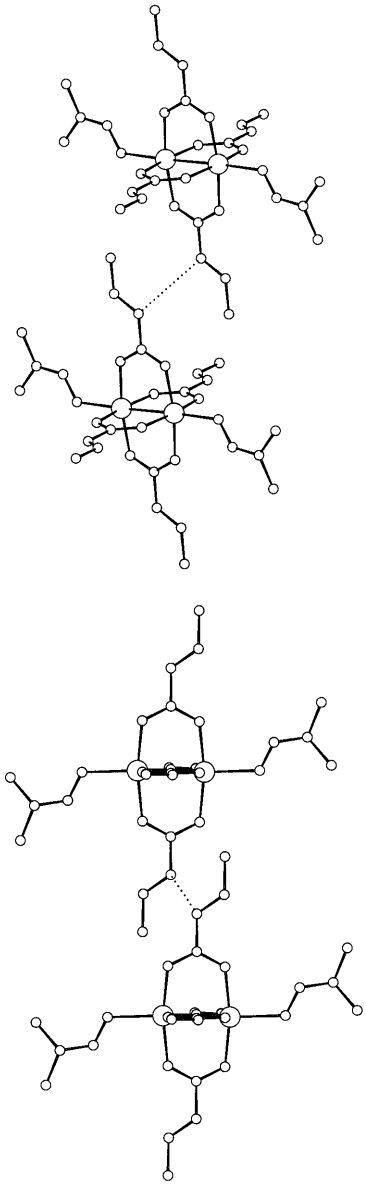

Fig. 2. Two molecules of $Cu_2(O_2CCH{=}CHCH_3)_4(DMF)_2$, showing (a) short Cα···Cα contacts of 3.611 Å (above) and (b) offset between double bonds, as projection onto the butenoate best planes (below).

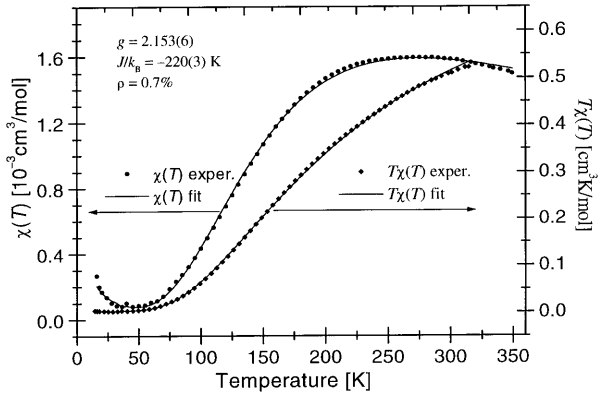

Fig. 3. Magnetic susceptibility $\chi(T)$ and $T\chi(T)$ measured in a powder sample of $Cu_2(O_2CCH{=}CHCH_3)_4(DMF)_2$ at a magnetic field of 0.1 T. Experimental points and fitting with Eq. (2).

3.2. Magnetic results

3.2.1. Magnetic susceptibility data

Fig. 3 displays the magnetic susceptibility $\chi(T)$ data observed with a magnetic field of 0.1 T, as a function of temperature T between 2 and 350 K. The Figure also displays the values of $T\chi(T)$. Considering the isotropic intradimeric exchange coupling with magnitude J [16]:

$$\mathscr{H}_{ex} = -J\mathbf{S}_A \cdot \mathbf{S}_B \quad (1)$$

the Bleaney and Bowers prediction [17] for the magnetic susceptibility of a mole (N) of dimers is:

$$\chi(T) = \frac{2Ng^2\mu_B^2}{k_B T[3+\exp(-J/k_B T)]}(1-\rho) + \frac{Ng^2\mu_B^2}{2k_B T}\rho \quad (2)$$

where g is the average g factor, k_B is the Boltzmann factor, and μ_B the Bohr magneton, is obtained for the magnetic susceptibility [16,18]. The second term in this expression accounts for the presence of a concentration ρ of uncoupled Cu(II) ions following a simple Curie law, and having the same g factor [18]. From the fit of Eq. (2) to the data in Fig. 3 we obtain:

$$g = 2.153 \pm 0.006,\ J/k_B = (-220 \pm 3)\ \text{K},\ \rho = 0.7\%$$

and the solid lines in Fig. 3 are obtained with these values. The intradimer interaction J is antiferromagnetic, and thus the copper dimer has a ground $S = 0$ singlet and an excited $S = 1$ triplet.

3.2.2. EPR data in powder samples

Fig. 4 shows the EPR spectrum of a powder sample obtained at 34.03 GHz and 293 K. The observed transitions occur only within the $S = 1$ triplet, as expected from the large value of J obtained from the susceptibility data. The powder spectrum reveals a nearly axial symmetry for the zero-field splitting [19]. The inset of Fig. 4 shows the field range of the spectrum corresponding to the $M = -1$ to $M = 1$ 'forbidden' transition within the triplet (half-field resonance). The shape

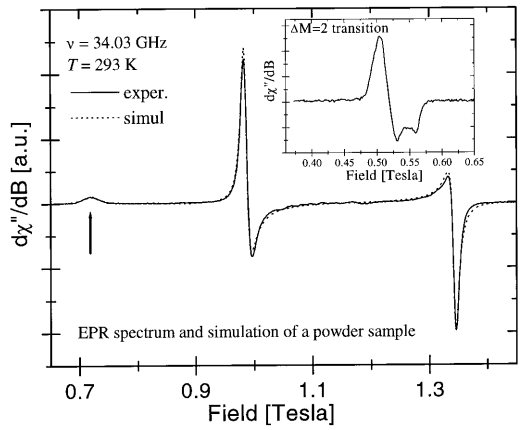

Fig. 4. EPR spectrum at 293 K of a powder sample of $Cu_2(O_2CCH{=}CHCH_3)_4(DMF)_2$. Experimental results and simulations with the parameters given in the text. The low-field peak, indicated by an arrow, displays a hyperfine splitting at low temperature.

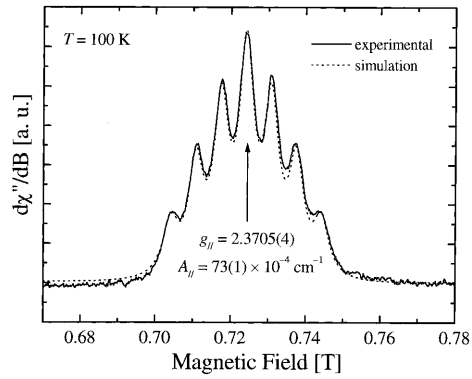

Fig. 5. EPR spectrum observed at 100 K in a powder sample of $Cu_2(O_2CCH{=}CHCH_3)_4(DMF)_2$ showing the hyperfine structure of the low-field resonance. The dashed line is a simulation of the spectrum obtained as indicated in the text.

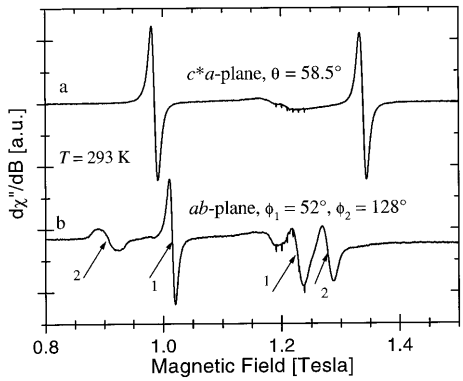

Fig. 6. EPR spectra of an oriented single crystal of $Cu_2(O_2CCH{=}CHCH_3)_4(DMF)_2$. (a) Magnetic field in the $zx = c^*a$ plane (perpendicular to the b axis), where all copper dimers are magnetically equivalent. (b) Magnetic field in the $xy = ab$ plane, where there are two non-equivalent (1 and 2) copper dimers. The resonances around 1.2 T are the cavity background.

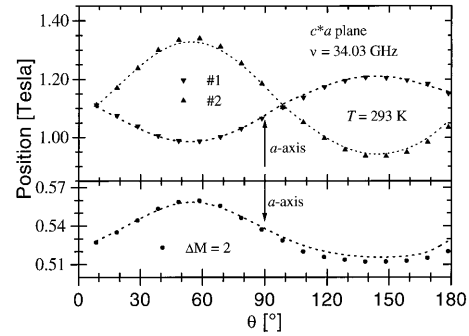

Fig. 7. Angular variation of the positions of the EPR lines observed in the $zx = c^*a$ plane (perpendicular to the b axis) of a single crystal of $Cu_2(O_2CCH{=}CHCH_3)_4(DMF)_2$. The upper part displays the data for the allowed $\pm 1 \leftrightarrow 0$ transitions within the spin triplet. The lower part displays the position of the 'forbidden' $-1 \leftrightarrow +1$ transition. The dotted lines are obtained with the fit described in the text.

of this absorption is a consequence of the anisotropy of the $\boldsymbol{g}$ tensor. The peaks of the spectrum shift and the integrated intensity decreases when the temperature is lowered as a consequence of the antiferromagnetic character of the intradimer exchange interaction. However, the resonances narrow and the resolution increases at lower T. At 100 K a hyperfine multiplet of seven lines due to the interaction of S with the $I = 3/2$ of the nuclear spins of the two copper ions is clearly observed (see Fig. 5) in the low-field region of the powder spectrum indicated with an arrow in Fig. 4.

3.2.3. EPR data in single-crystal samples

EPR spectra of a single-crystal sample were obtained with the magnetic field at 10° intervals in each of the three orthogonal planes *ab*, *c*a* and *c*b* of the sample at 293 K. For a general orientation of the applied magnetic field, the spectrum displays two symmetry-related fine structure groups of three resonances attributed to the two symmetry-related dimers in the unit cell. For **B** along the b axis or in the ac^* plane these two groups collapse to one, as expected by symmetry arguments. Fig. 6(a, b) display typical spectra chosen from our data. The positions of the resonances were determined as a function of magnetic-field orientation and the results in the three studied planes are displayed in Figs. 7–9. The upper part of these figures include the field range where the allowed $M = \pm 1 \leftrightarrow M = 0$ transitions occur. The lower part includes the field range for the forbidden resonance $M = +1 \leftrightarrow M = -1$. For simplicity we include in these Figures only the resonances corresponding to one copper dimer in the unit cell.

The spin Hamiltonian describing the spectra of the spin triplet ($S = 1$ state) for a homonuclear dimer having a center of symmetry is [20]:

$$\mathcal{H}_s = \mu_B \mathrm{S} \cdot \boldsymbol{g} \cdot \mathbf{B} + \mathrm{S} \cdot \boldsymbol{D} \cdot \mathrm{S} \qquad (3)$$

The $\boldsymbol{g}$ tensor of Eq. (3) is identical for the two copper ions. $\boldsymbol{D}$ is a symmetric and traceless zero-field splitting tensor responsible of the splitting of the spin triplet, and arising from anisotropic exchange and dipole–dipole interactions [19]. It has five independent components which may be described by two parameters (D and E) describing the diagonal axial (D) and orthorhombic (E) components [20], plus three angles giving the eigenvectors of the tensor in the experimental coordinate system. D and E are related to the principal components of D by:

$$\mathrm{D} = D_{zz} - 1/2(D_{xx} + D_{yy}),\ \mathrm{E} = 1/2(D_{xx} - D_{yy}) \qquad (4)$$

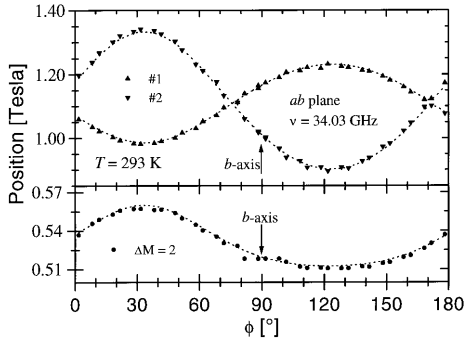

Fig. 8. Angular variation of the positions of the EPR lines observed in the $xy = ab$ plane of a single crystal of $Cu_2(O_2CCH{=}CHCH_3)_4(DMF)_2$. Only the resonances corresponding to one copper dimer are shown. The upper part displays the data for the allowed $\pm 1 \leftrightarrow 0$ transitions within the spin triplet. The lower part displays the position of the 'forbidden' $-1 \leftrightarrow +1$ transition. The dotted lines are obtained with the fit described in the text.

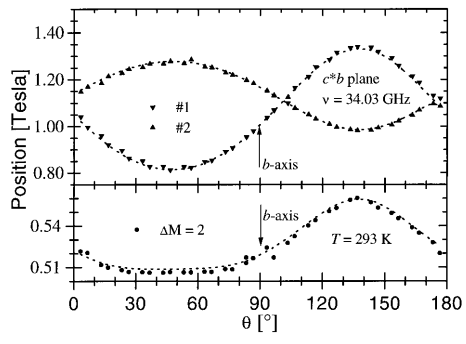

Fig. 9. Angular variation of the positions of the EPR lines observed in the $zy = c^*b$ plane of a single crystal of $Cu_2(O_2CCH{=}CHCH_3)_4(DMF)_2$. Only the resonances corresponding to one copper dimer are shown. The upper part displays the data for the allowed $\pm 1 \leftrightarrow 0$ transitions within the spin triplet. The lower part displays the position of the 'forbidden' $-1 \leftrightarrow +1$ transition. The dotted lines are obtained with the fit described in the text.

Table 3
Values of the components and eigenvalues of the $\boldsymbol{g}$ and $\boldsymbol{D}$ tensors obtained from the single-crystal EPR results at 293 K for one of the copper dimers in the unit cell

Component	$\boldsymbol{g}$ tensor	$\boldsymbol{D}$ tensor (GHz)
xx	2.128	1.410
yy	2.203	−1.063
zz	2.184	−0.347
xy	−0.083	2.936
xz	−0.074	2.676
yz	0.119	−4.030
Eigenvalues		
1	2.0735(12)	3.360(5)
2	2.0769(12)	3.339(5)
3	2.3648(12)	−6.698(4)

The parameters in Eq. (3) were obtained by fitting the spin Hamiltonian to the data in Figs. 7–9 using the simulated annealing method [21] that has been described previously [22–24]. There are two possibilities of associating the resonances observed in the $xy = ab$ and $yz = bc^*$ planes with certain transitions. Each gives rise to a different set of spin Hamiltonian parameters. However, one of them has no physical meaning because it does not reproduce the powder spectrum of Fig. 4, and was therefore discarded. The values of the components of the $\boldsymbol{g}$ and $\boldsymbol{D}$ tensors in the $xyz = abc^*$ coordinate system calculated from the meaningful data set are given in Table 3, together with their eigenvalues. Using the eigenvalues of the $\boldsymbol{D}$ tensor and Eq. (4) we obtain:

$$\mathrm{D} = -10.04(1)\ \mathrm{GHz}\ \text{and}\ \mathrm{E} = 0.01(1)\ \mathrm{GHz}$$

The $\boldsymbol{g}$ and $\boldsymbol{D}$ tensors have an approximately axial symmetry, and consequently the uncertainty of the orientations of the eigenstates in the plane perpendicular to the axis are very large. The axial directions of $\boldsymbol{g}$ and $\boldsymbol{D}$ are the same within 1.5°, and in excellent agreement with the direction connecting the copper ions in the dimer obtained from the crystal structure. The other two principal directions of $\boldsymbol{g}$ and $\boldsymbol{D}$ are not coincident. The values given in Table 3 were used to simulate the powder EPR spectrum in order to produce the dashed line in Fig. 4.

The principal g values of $Cu_2(O_2CCH{=}CHCH_3)_4(DMF)_2$ given in Table 3 are very similar to those observed in similar carboxylate-bridged copper dimers where the Cu(II) ions are coordinated by a square of O ligands and there is a center of symmetry between the copper ions.

There are two contributions to the observed zero-field splitting of the spin triplet. One is due to the dipole–dipole interaction between the unpaired spins in the two copper atoms. The other is provided by the so-called anisotropic exchange, and arises from the spin–orbit interaction.

In the simplest point charge approach the dipolar contribution can be written as [25]:

$$\mathrm{S}_1 \cdot D_{\mathrm{dip}}(1,2) \cdot \mathrm{S}_2 = \{\mu_1 \cdot \mu_2 - 3(\mu_1 \cdot \boldsymbol{r})(\mu_2 \cdot \boldsymbol{r})\}/\mathbf{R}^3 \qquad (5)$$

where $\boldsymbol{r} = \mathbf{R}/|\mathbf{R}|$, and $\mathbf{R}$ is the vector connecting the copper ions. The magnetic moments can be written as

$\mu_1 = -\mu_B \boldsymbol{g} \cdot S_1$ and $\mu_2 = -\mu_B \boldsymbol{g} \cdot S_2$. Replacing these values (Table 3) in Eq. (5) and using the definitions of D and E:

$D_{dip}/h = -5.64$ GHz and $E_{dip} \approx 0$

The magnitude of the contribution of the anisotropic exchange to D and E may be calculated by subtracting the dipolar contribution to the experimental result. Considering the Cu–Cu distance, and the size of the unpaired electron distribution of Cu, the point dipolar approximation for D_{dip} should be considered a minimum value. Thus, the value

$D_{an.\ exch.}/h \approx -4.4$ GHz

should be considered an upper limit for the magnitude of the anisotropic exchange contribution.

Fig. 5 displays the hyperfine structure of the dimer measured at 100 K in the region of the spectrum where $g = g_{//} \approx 2.37$. The multiplicity (seven lines) and relative intensity (1:2:3:4:3:2:1) of this structure clearly indicates the dimeric character of the spectrum. The sum of seven Lorentzian-shaped resonances was fitted to the low-field part of the powder spectrum at 100 K to give a splitting of 66(1) Gauss, and peak-to-peak line widths of 28 Gauss. Thus, the hyperfine splitting observed along the direction of $g \approx g_{//}$ where the splitting is largest, 73×10^{-4} cm^{-1}, would indicate $A_{//} = 146(2) \times 10^{-4}$ cm^{-1} for single copper ions.

4. Concluding remarks

We have synthesized and structurally characterized a new dimeric copper compound with unsaturated ligands. Irradiation of this complex with γ-rays did not produce a dimeric product, as might be expected from the short contacts observed between pairs of molecules related by a center of symmetry. However, since metal complexes of unsaturated carboxylates often show unusual solid-state reactivity, it is always important to carefully examine examples where short contacts occur between the unsaturated centers. Although no reactivity has been observed in the present case, the geometrical information provided opens an initial structural database for a putative ene dimerization in the solid state. Geometric criteria for a solid-state ene dimerization have not yet been established. The only published example, deduced from the unit cell dimensions of **1**, leads to an estimated C···C contact distance of 3.47 Å. However, the intermolecular orientation remains unknown [2]. Further studies of this kind, where a number of related structures are produced in order to vary the C···C contact distance and orientation, should be helpful in both the discovery of new reactive phases, as well as the elucidation of criteria for new types of solid-state reactivity.

A detailed magnetic characterization including magnetic susceptibility and single-crystal EPR measurements have been performed. The value $J/k_B = (-220 \pm 3)$ K obtained from the susceptibility data for the exchange coupling between the two copper ions at $d = 2.613$ Å in $Cu_2(O_2CCH{=}CHCH_3)_4(DMF)_2$ is smaller than the values $J/k_B = -296$ K in copper acetate monohydrate [18] ($d = 2.64$ Å) or J/k_B between -285 and -305 K measured in various similar copper dimers in complexes of Cu(II) with indomethacin ($d \approx 2.63$ Å) [26].

The values $D/h = -10.04(1)$ GHz and $E/h = 0.01(1)$ GHz obtained from the EPR data for the zero-field splitting of the excited triplet are analyzed in terms of dipolar interactions between copper neighbors, and anisotropic contributions to the exchange interaction. The hyperfine splittings of the EPR spectra reflect the dimeric character of the compound.

Acknowledgements

B.M.F. thanks the National Science Foundation for a grant (DMR-9629994) in the partial support of this research. M.P. and R.C. are members of CONICET, Argentina.

References

[1] (a) K. Naruchi, S. Tanaka, M. Yamamoto, K. Yamada, Nippon Kagaku Kaishi (1983) 1291. (b) K. Naruchi, M. Miura, J. Chem. Soc., Perkin Trans. 2 (1987) 113.
[2] G.C.D. Delgado, K.A. Wheeler, B.B. Snider, B.M. Foxman, Angew. Chem., Int. Ed. Engl. 30 (1991) 420.
[3] T.H. Cho, B. Chaudhuri, B.B. Snider, B.M. Foxman, J. Chem. Soc., Chem. Commun. (1996) 1337.
[4] B.M. Foxman, J.D. Jaufmann, J. Polym. Sci, Polym. Symp. 70 (1983) 31.
[5] J.W. Shepherd, III, B.M. Foxman, Mol. Cryst. Liq. Cryst. 137 (1986) 87.
[6] (a) M.D. Cohen, G.M.J. Schmidt, J. Chem. Soc. (1964) 1996. (b) F.L. Hirshfeld, G.M.J. Schmidt, J. Polym. Sci., Part A 2 (1964) 2181.
[7] F.H. Allen, O. Kennard, Chem. Design Automat. News. 8 (1993) 1 and 31.
[8] M. Bukowska-Strzyzewska, J. Skoweranda, E. Heyduk, J. Mrozinski, Inorg. Chim. Acta 73 (1983) 207.
[9] E.B. Shamuratov, A.S. Batsanov, Kh.T. Sharipov, Yu.T. Struchkov, T. Azizov, Koord. Khim. 20 (1994) 754.
[10] C.A. Booth, B.M. Foxman, J.D. Jaufmann, in: D.J. Sandman (Ed.), Crystallographically Ordered Polymers, ACS Symposium Series 337, American Chemical Society, Washington, DC, 1987, pp. 95–105.
[11] L.H. Straver, CAD4-EXPRESS, Enraf–Nonius, Delft, The Netherlands, 1992.
[12] C.K. Fair, MolEN, An Interactive Structure Solution Procedure, Enraf–Nonius, Delft, The Netherlands, 1990.
[13] D.J. Watkin, C.K. Prout, J.R. Carruthers, P.W. Betteridge, CRYSTALS, Issue 10, Chemical Crystallography Laboratory, University of Oxford, Oxford, 1996.

[14] D.J. Watkin, C.K. Prout, L.J. Pearce, CAMERON, Chemical Crystallography Laboratory, University of Oxford, Oxford, 1996.
[15] S.K. Kearsley, in: G.R. Desiraju (Ed.), Organic Solid State Chemistry, Elsevier, Amsterdam, 1987, pp. 69–113.
[16] R.L. Carlin, Magnetochemistry, Springer, Berlin, 1986.
[17] B. Bleaney, K.D. Bowers, Proc. R. Soc. (London) Ser. A 214 (1952) 451.
[18] O. Kahn, Molecular Magnetism, VCH, New York, 1993.
[19] A. Bencini, D. Gatteschi, Electron Paramagnetic Resonance of Exchange Coupled Systems, Springer, Berlin, 1990.
[20] N.M. Atherton, Principles of Electron Spin Resonance, Horwood, New York, 1993.
[21] S. Kirkpatrick, C.D. Gelatt, M.P. Vecchi, Science 220 (1983) 671.
[22] W.H. Press, S.A. Teukolsky, W.T. Vetterling, B.P. Flannery, Numerical Recipes in FORTRAN: The Art of Scientific Computing, Cambridge University Press, New York, 1992.
[23] A. Aarts, J. Korst, Simulated Annealing and Boltzmann Machines. A Stochastic Approach to Combinatorial Optimization and Neural Computing, Wiley, New York, 1989.
[24] R. Calvo, E.C. Abresch, R. Bittl, G. Feher, W. Hofbauer, R.A. Isaacson, W. Lubitz, M.Y. Okamura, M.L. Paddock, J. Am. Chem. Soc. 122 (2000) 7327 (This is a recent application of the simulated annealing method to fitting of EPR spectra).
[25] A. Ozarowski, D. Reinen, Inorg. Chem. 25 (1986) 1704.
[26] J.E. Weder, W.H. Hambley, B.J. Kennedy, P.A. Lay, D. MacLachlan, R. Bramley, C.D. Delfs, K.S. Murray, B. Moubaraki, B. Warwick, J.R. Biffin, H.L. Regtop, Inorg. Chem. 38 (1999) 1736.